AGU ADVANCING EARTH AND SPACE SCIENCE

Geophysical Research Letters

RESEARCH LETTER
10.1029/2020GL090431

The Rheological Behavior of CO_2 Ice: Application to Glacial Flow on Mars

A. J. Cross[1,2], D. L. Goldsby[1], T. F. Hager[1], and I. B. Smith[3,4]

[1]Department of Earth and Environmental Science, University of Pennsylvania, Philadelphia, PA, USA, [2]Department of Geology and Geophysics, Woods Hole Oceanographic Institution, Woods Hole, MA, USA, [3]Lassonde School of Engineering, York University, Toronto, Ontario, Canada, [4]Planetary Science Institute, Lakewood, CO, USA

Key Points:
- Laboratory experiments reveal highly nonlinear ($n = 8$) creep of CO_2 ice at high stresses, corroborating previous findings
- We discover linear viscous ($n = 1$), grain size sensitive creep of CO_2 ice at low stresses, interpreted as the diffusion creep regime
- The extreme nonlinearity of CO_2 ice creep facilitates the glacial flow and ponding of massive CO_2 ice deposits at Mars's south pole

Supporting Information:
- Supporting Information S1

Correspondence to:
A. J. Cross,
across@whoi.edu

Citation:
Cross, A. J., Goldsby, D. L., Hager, T. F., & Smith, I. B. (2020). The rheological behavior of CO_2 ice: Application to glacial flow on Mars. *Geophysical Research Letters*, *47*, e2020GL090431. https://doi.org/10.1029/2020GL090431

Received 20 AUG 2020
Accepted 26 OCT 2020
Accepted article online 29 OCT 2020

Abstract Vast quantities of solid CO_2 reside in topographic basins of the south polar layered deposits (SPLD) on Mars and exhibit morphological features indicative of glacial flow. Previous experimental studies showed that CO_2 ice is 1–2 orders of magnitude weaker than water ice under Martian polar conditions. Here we present data from deformation experiments on pure, fine-grained CO_2 ice, over a broader range of temperatures than previously explored (158–213 K). The experiments confirm previous observations of highly nonlinear power law creep at larger stresses, but also show a transition to a previously unseen linear-viscous creep regime at lower stresses. We examine the viscosity of CO_2 within the SPLD and predict that the CO_2-rich deposits are modestly stronger than previously thought. Nevertheless, CO_2 ice flows much more readily than H_2O ice, particularly on the steep flanks of SPLD topographic basins, allowing the CO_2 to pond as observed.

Plain Language Summary Massive deposits of solid CO_2 (dry ice) were recently discovered at Mars's south pole and appear to be flowing like glaciers on Earth. To predict the glacial flow rate of dry ice at Martian polar conditions, we produced and then deformed samples of CO_2 ice in the laboratory. Under relatively large stresses and low temperatures, the rate of CO_2 ice flow is very sensitive to changes in stress, meaning that dry-ice glaciers will flow much faster over steep topographic slopes at Mars's south pole than over shallow slopes. This extreme sensitivity to the slope of underlying topography explains why CO_2 ice deposits are ponded within topographic basins at Mars's south pole, preserving a half-million-year long climate record.

1. Introduction

Mars's south pole is covered by the perennial south polar residual cap (SPRC) that extends across an area of up to 90,000 km^2 (Thomas et al., 2009) (Figure 1a) and overlies the larger, dome-shaped south polar layered deposits (SPLD), which are ≤3.7 km thick at Mars's south pole (Plaut et al., 2007). The composition of the SPRC has been studied extensively. Early workers detected infrared spectra for solid carbon dioxide at Mars' south pole, and hypothesized that the entirety of the SPRC and SPLD could be composed of CO_2 (Chase et al., 1972; Herr & Pimentel, 1969). This hypothesis prompted investigations into the material properties of CO_2 ice (Clark & Mullin, 1976) and led to speculation that there could be basal melting of the CO_2-rich deposits (Sagan, 1973). To examine the potential for glacial flow of the SPLD, Clark and Mullin (1976) and Durham et al. (1999) performed experiments to determine the rheological behavior of CO_2 ice. Both studies concluded that CO_2 ice is 1–2 orders of magnitude weaker than water ice of comparable grain size (at the same stress and temperature). More recently, Kaufmann et al. (2020) performed indentation tests to determine the hardness and yield strength of CO_2 and H_2O ices at Martian temperatures, finding CO_2 ice to be slightly weaker than H_2O ice, although their experiments were performed at relatively large loads in order to investigate the fracturing and plasticity behavior of CO_2 ice, rather than the viscous creep responsible for glacial flow. By incorporating the creep properties of CO_2 and H_2O ices into a model of gravitational spreading, Nye et al. (2000) found that a CO_2 ice cap would too easily collapse under its own weight and could not, therefore, maintain the observed >3 km thickness of the SPLD over their estimated age of 10^7–10^8 years (Herkenhoff & Plaut, 2000). Nye et al. thus concluded that glacial flow of the SPLD must be governed by the creep behavior of H_2O ice, not CO_2 ice.

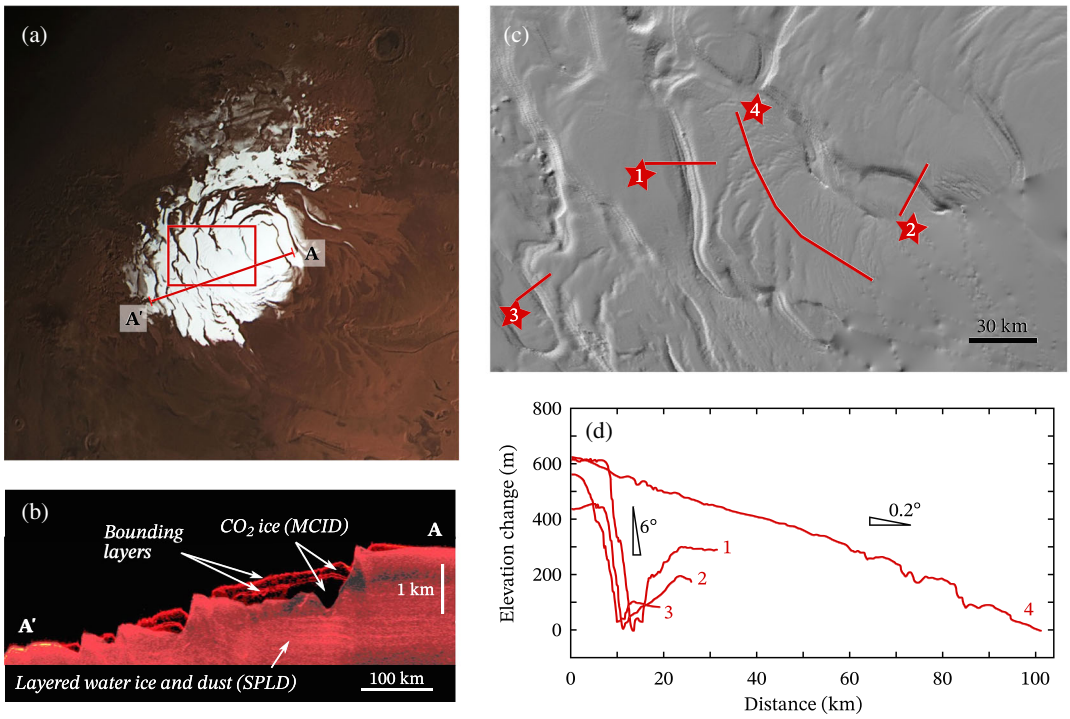

Figure 1. (a) Mars's south pole, viewed from the high-resolution stereo camera onboard the Mars Express orbiter. (b) A shallow radar cross section of the SPLD (transect A–A' in (a)), after Bierson et al. (2016). (c) Hillshade map from the Mars Orbiter laser altimeter instrument on the Mars Global Surveyor spacecraft (boxed region in (a)). (d) Surface topography profiles across the south polar ice cap. Topographic depressions within the SPLD (transects 1–3) have steep flanking slopes (≥6°) and are presently filled with CO_2 ice. Down-glacier slopes (transect 4) are significantly shallower (<0.5°).

3Such was the state of knowledge until shallow radar (SHARAD) soundings from the Mars Reconnaissance Orbiter revealed the presence of deep, reflection-free deposits contained within topographic basins at the top of the SPLD (Bierson et al., 2016; Phillips et al., 2011) (Figure 1b). From the analysis of dielectric permittivity data, it was determined that as much as 1% of the SPLD is composed of massive CO_2 ice deposits (MCID)—up to 1-km thick in places—that have accumulated during periods of atmospheric collapse over the past ~500 kyr (Manning et al., 2019). Furthermore, there is growing evidence for glacial flow of the MCID, including a strong correlation between the locations of the thick CO_2 deposits (Putzig et al., 2018) and morphological features reminiscent of terrestrial glaciation (Clark & Mullin, 1976). These new observations call for a reexamination of the creep properties of CO_2 ice.

New experiments exploring the creep behavior of CO_2 ice are warranted for several reasons. First, the experiments of Clark and Mullin (1976) were performed with relatively poor temperature control and on unconfined samples. A lack of confinement may have allowed sample microcracking, which would explain the relative weakness of their samples compared with those of Durham et al. (1999), deformed at elevated confining pressures. Second, both experimental studies were performed on commercial-grade dry ice containing trace amounts of propylene glycol (0.02 vol.%) and oil (0.001 vol.%) (Durham et al., 1999). These impurities may have influenced the deformation behavior of the fabricated samples. Third, with the recent discovery of the MCID—which are up to 1 km in thickness (Bierson et al., 2016; Phillips et al., 2011)—south polar CO_2 ices are likely subjected to cryostatic pressures of up to 5.5 MPa, enough to stabilize solid CO_2 up to a melting temperature of ~218 K. Previous experimental studies did not explore conditions above the 1-atm sublimation temperature of solid CO_2 (194.5 K); thus, it remains to be seen whether the creep behavior of CO_2 ice changes markedly within 20° of its melting point due to equilibrium premelting (Alsayed et al., 2005; Dash et al., 1995) or other forms of "premonitory melting" that result from increased subsolidus grain boundary disorder (Dash et al., 2006; Luo & Chiang, 2008; Marquardt & Faul, 2018). Lastly, neither previous study explored the rheological behavior of fine-grained (<100 μm) CO_2 ice—experiments in both studies

were conducted on samples with grain sizes of ~250 μm or larger. Under small stresses, fine-grained crystalline materials commonly deform by grain-size-sensitive (GSS) creep mechanisms involving grain boundary sliding accompanied by lattice diffusion, grain boundary diffusion, or dislocation motion (Frost & Ashby, 1982). However, GSS creep has never been observed for CO_2 ice. This study was predicated, in part, on the possibility that, by fabricating samples of fine grain size, we might observe GSS creep in CO_2 ice at laboratory strain rates. GSS creep often dominates in low stress regions of terrestrial ice sheets (e.g., Goldsby, 2006; Kuiper et al., 2020) and, thus, may contribute to glacial flow of the SPLD.

2. Experimental Methods

2.1. Starting Material

Fine-grained, high-purity powders of solid CO_2 were synthesized by filling a sealed Perspex chamber with CO_2 gas (Figure S1 in the supporting information). Inside the chamber, a 25.4-mm-thick aluminum plate —half submerged in liquid nitrogen (LN_2)—was cooled sufficiently to enable the accumulation of CO_2 powder deposited directly from the gas phase in the chamber. Positive N_2 (from the boiling LN_2) and CO_2 gas pressures prevented atmospheric H_2O from entering the chamber and contaminating the CO_2 powders. Sublimation of the CO_2 powders produced no visible liquid water, suggesting a powder purity of >99%. Powders were packed into a thin-walled indium tube ("jacket") with a 25.4-mm internal diameter, sealed at one end by melting the jacket against a copper-plated steel end-cap. The other end of the jacket was melted against a steel semiinternal force gauge, while the jacketed sample was immersed in LN_2 to prevent sublimation of the packed CO_2 powders.

Jacketed samples were isostatically "hot" pressed in a cryogenic gas medium apparatus at experimental run conditions (i.e., at a confining pressure $P = 10$ MPa and a temperature T in the range 158–213 K). For experiments conducted above the 1-atm CO_2 sublimation temperature, 194.5 K, samples were pressurized to 1 MPa within 2–3 min of loading them into the pressure vessel to prevent sublimation. At a confining pressure of 1 MPa, solid CO_2 is stable up to a melting temperature of 216.3 K. Hot-pressing consistently produced 10–20% compaction, measured both by the change of the "hit-point"—that is, the position at which the deformation piston made physical contact with the bottom of the sample—during pressurization, and by extracting some samples from the pressure vessel for direct measurements after hot pressing. No measurable compaction was achieved above a confining pressure of 10 MPa, indicating negligible porosity.

Particle sizes of the CO_2 powders were determined using an optical microscope, with the powders immersed in LN_2 in a Petri dish. Images taken rapidly—before evaporation of the LN_2 and sublimation of the powders —revealed equant particles with a geometric mean particle size of ~30 μm (Figure S2).

2.2. Deformation Experiments

Experiments were performed in the same cryogenic gas medium apparatus used by Durham et al. (1999), in which the pressure vessel is cooled by immersion in a chilled alcohol bath (see Heard et al., 1990, for details). After hot pressing, each sample was left for roughly 1 hr to thermally equilibrate with the apparatus, then subsequently deformed in uniaxial compression under a constant displacement rate (i.e., at a nominally constant strain rate) to strains of ≤20%. Stress and strain rate data were used to characterize the rheological behavior of CO_2 ice, assuming the following power law relationship:

$$\dot{\varepsilon} = A\sigma^n d^{-m} \exp\left(\frac{-Q}{RT}\right), \tag{1}$$

where $\dot{\varepsilon}$ is strain rate, A is a constant, σ is differential stress, d is grain size, Q is the activation energy for creep, R is the gas constant, and n and m are the stress and grain size exponents, respectively.

Stresses were corrected for the increasing cross-sectional area of the sample during deformation (assuming constant sample volume), and for the strength of the indium jacket. The resolution of the stress measurements is ±0.1 MPa, limited primarily by thermal drift of the apparatus (±0.5 K). Only steady-state (i.e., strain-invariant) stresses were used to derive the flow law parameters. Example stress-strain curves are provided in Figure S3.

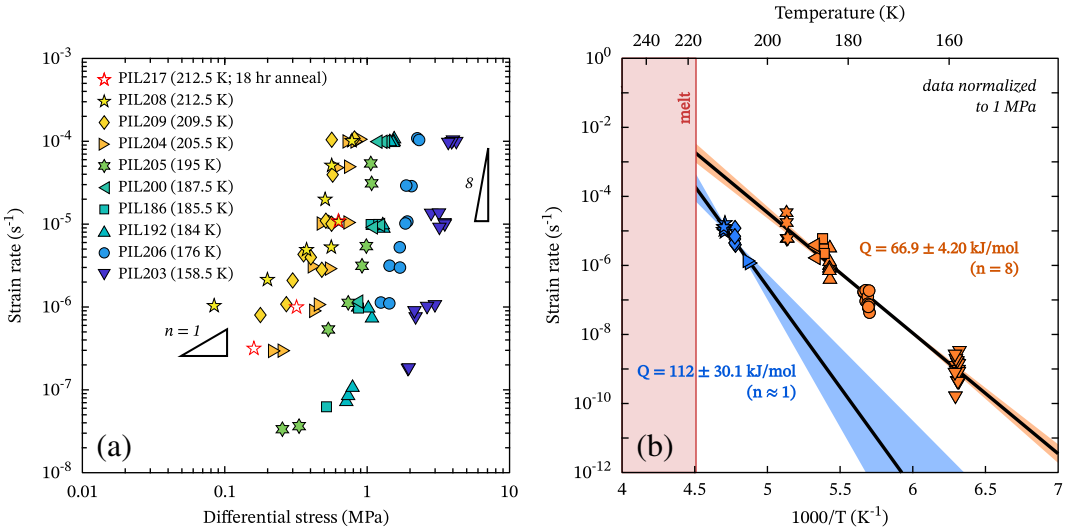

Figure 2. (a) Strain rate versus differential stress. Data points are colored by temperature. (b) Strain rate versus inverse temperature for the high-stress ($n = 8$; orange points) and low-stress ($n \approx 1$; blue points) data. Shaded regions represent the 95% confidence intervals of each linear regression (black lines).

3. Results

We performed nine constant-temperature, strain rate-stepping experiments over the temperature range 158–213 K. During each test, several steps in the range 10^{-8}–10^{-4} s^{-1} were imposed in order to determine the stress exponent n.

The steady-state data reveal two distinct deformation regimes in $\log_{10} \dot{\varepsilon}$ versus $\log_{10} \sigma$ space (Figures 2a and S4). At low temperatures and high stresses, the data fall on a linear trend described by a slope (i.e., stress exponent, n) of 8.0 ± 2.2. With increasing temperature and decreasing stress, n decreases until a second linear trend emerges with $n = 1.1 \pm 0.53$. This low stress, $n \approx 1$ regime is observed only in our high-temperature (>195 K) experiments—territory not explored by either Clark and Mullin (1976) or Durham et al. (1999).

To derive activation energies for creep in these two deformation regimes, we performed a linear regression of the data in log $\dot{\varepsilon}$ versus $1/T$ space, where the slope is equal to $-Q/R$ (Figure 2b). The low stress ($n \approx 1$) data yield an activation energy of $Q = 112 \pm 30.1$ kJ/mol, whereas the high stress ($n = 8$) data give $Q = 66.9 \pm 4.20$ kJ/mol. Flow law parameters are summarized in Table 1, along with those from Clark and Mullin (1976) and Durham et al. (1999) for comparison. For reasons outlined below, we have omitted the constitutive parameters for the low stress $n \approx 1$ regime from Table 1.

4. Discussion

4.1. Deformation Regimes

4.1.1. High-Stress Regime

We can resolve at least two distinct creep regimes for CO_2 ice, described by stress exponent values of $n = 8$ and $n \approx 1$ (Figure 2a). The high-stress regime, where $n = 8$, is equivalent to that explored in both previous experimental studies of CO_2 ice deformation, although we obtain a larger stress exponent: Clark and Mullin (1976) reported $n = 3.9$, whereas Durham et al. (1999) found $n = 5.6$. However, Clark and Mullin's experiments were performed over a relatively narrow range of conditions ($T = 163$–193 K; $\dot{\varepsilon} = 2 \times 10^{-7}$ to 2×10^{-5} s^{-1}). Over the same range of conditions, we too find lower apparent values of n (Figure S4). Furthermore, Durham et al. (1999) reported a modest amount of sample-to-sample variation in their study and found that their data could be fit equally well by a stress exponent as large as 7 (Nye et al., 2000—see Table 1).

The stress sensitivity in the high-stress regime ($n = 8 \pm 2$) is greater than that anticipated for deformation rate-limited by either grain boundary

Table 1
Flow Law Parameters for CO_2 Ice

Reference	$\log_{10}A$ (MPa^{-n} s^{-1})	Q (kJ/mol)	n	m
Clark and Mullin (1976)	10.5	51	3.9	0
Durham et al. (1999)	3.86	33	5.6	0
Nye et al. (2000)[a]	11.1	59	7.0	0
This study	13.0 ± 1.27	66.9 ± 4.20	8.0 ± 2.2	0

Note. Errors give the 95% confidence intervals (~2σ).
[a]Alternative fit through the data of Durham et al. (1999).

sliding ($n \approx 2$) or dislocation climb ($n = 3$–4.5) (Poirier, 1985, pp. 111). Other candidate deformation mechanisms include dislocation creep controlled by (1) pipe diffusion along dislocation cores, (2) cross-slip, (3) jogged screw dislocations, or (4) lattice resistance during dislocation glide (de Bresser, 2002). Pipe-diffusion-controlled creep can result in power law stress exponents of 5–7 or greater (Ruano et al., 1981), but typically becomes rate controlling only at homologous temperatures (T/T_m) below 0.6 (see Luthy et al., 1980)—that is, at $T < 130$ K for CO_2 ice—due to the relatively low activation energy for pipe diffusion (Poirier, 1985, pp. 50). However, for materials in which lattice self-diffusion is sluggish, pipe diffusion can remain important to relatively high temperatures, as is thought to be the case for olivine (Hirth & Kohlstedt, 2015) and tin (Sherby & Weertman, 1979). In the absence of self-diffusion data for CO_2 ice, we therefore cannot rule out pipe diffusion as an important rate-controlling process for power law CO_2 ice creep.

Creep controlled by either cross-slip, jogged screw dislocations, or lattice resistance, on the other hand, is best described by an exponential law yielding an increase in the apparent stress exponent, n' ($\delta \ln \dot{\varepsilon} / \delta \ln \sigma$), with increasing strain rate. Exponential flow laws for these various mechanisms have previously been used to explain the creep behavior of calcite (de Bresser, 2002; Renner & Evans, 2002), which exhibits an increase in n' from 3 to 8 with increasing stress (Renner et al., 2002). Given the apparent increase in n with stress observed here (Figure S4), we have also fit our high-stress data to these various exponential laws (Figure S5). Without constraints on the dislocation types and active slip systems for solid CO_2, it is not possible to determine which exponential creep law is most appropriate. However, a Peierls law for dislocation glide limited by lattice friction provides the most satisfying fit through the data (i.e., the fit with the smallest root-mean-square (RMS) error—Figure S5) and is defined as

$$\dot{\varepsilon}_p = A_p \sigma^2 \exp\left(-\frac{Q_p}{RT}\left[1 - \left(\frac{\sigma}{\sigma_p}\right)^p\right]^q\right) \quad (2)$$

where the Peierls stress, σ_p, is the resistance to dislocation glide at 0 K (Weertman, 1957). The parameters A_p, Q_p, and σ_p were obtained simultaneously via nonlinear least-squares regression in the MATLAB Curve Fitting toolbox. To reduce the number of degrees of freedom, the regression was performed with various combinations of the exponents p and q, which can vary between 0–1 and 1–2, respectively (Frost & Ashby, 1982). Values of $p = 1/3$ and $q = 2$ were adopted, as these values minimized the RMS error of the regression (Figure S6), yielding $Q_p = 93.5 \pm 9.95$ kJ/mol and $\sigma_p = 503 \pm 78.6$ MPa. Note, however, that the best fit p and q values are those that produce an exponential fit closely resembling a power law fit. Furthermore, the RMS error obtained using the Peierls law is larger than that obtained using a power law (Figure S5). Thus, we suggest that a power law fit is most suitable, with the region of increasing n' representing a transition between $n = 1$ and $n = 8$ power law creep.

4.1.2. Low-Stress Regime

At low stresses and high temperatures, we observe a linear relationship ($n \approx 1$) between stress and strain rate (Figure 2a) which has not been observed before for CO_2 ice. Linear-viscous behavior is commonly associated with diffusion creep, but may also arise from Harper-Dorn creep—an enigmatic deformation mechanism where dislocation density is independent of differential stress (see Kumar et al., 2007). However, whereas the strain rate arising from diffusion creep exhibits a grain size dependence ($\dot{\varepsilon} \propto d^{-m}$), Harper-Dorn creep is grain size insensitive.

To distinguish between these two deformation mechanisms, we performed an experiment on a coarser-grained CO_2 ice sample produced by annealing a fine-grained sample for 18 hr before deforming it. In the $n \approx 1$ regime, we measured stresses up to 5 times larger for the coarse-grained sample than for a fine-grained sample deformed at the same temperature and strain rate (Figures 2a and S7). In the $n = 8$ regime, however, the fine- and coarse-grained samples have similar strengths. These results indicate that deformation within the $n \approx 1$ regime is grain-size-sensitive, and likely due to diffusion creep, whereas the $n = 8$ regime is grain-size-insensitive. Experiments to fully determine a diffusion creep ($n = 1$) flow law for CO_2 ice—namely the grain size exponent, m—will be the focus of a future study, as grain size measurements of dense CO_2 samples have thus far proved difficult to obtain. Furthermore, extrapolation to Martian conditions will require constraints on CO_2 grain sizes within the MCID. Current best estimates for CO_2 grain sizes within the MCID are provided by grain size estimates for the overlying and relatively young SPRC deposits, which have reflectance spectra best fit by a model with 4.25-mm diameter CO_2 grains

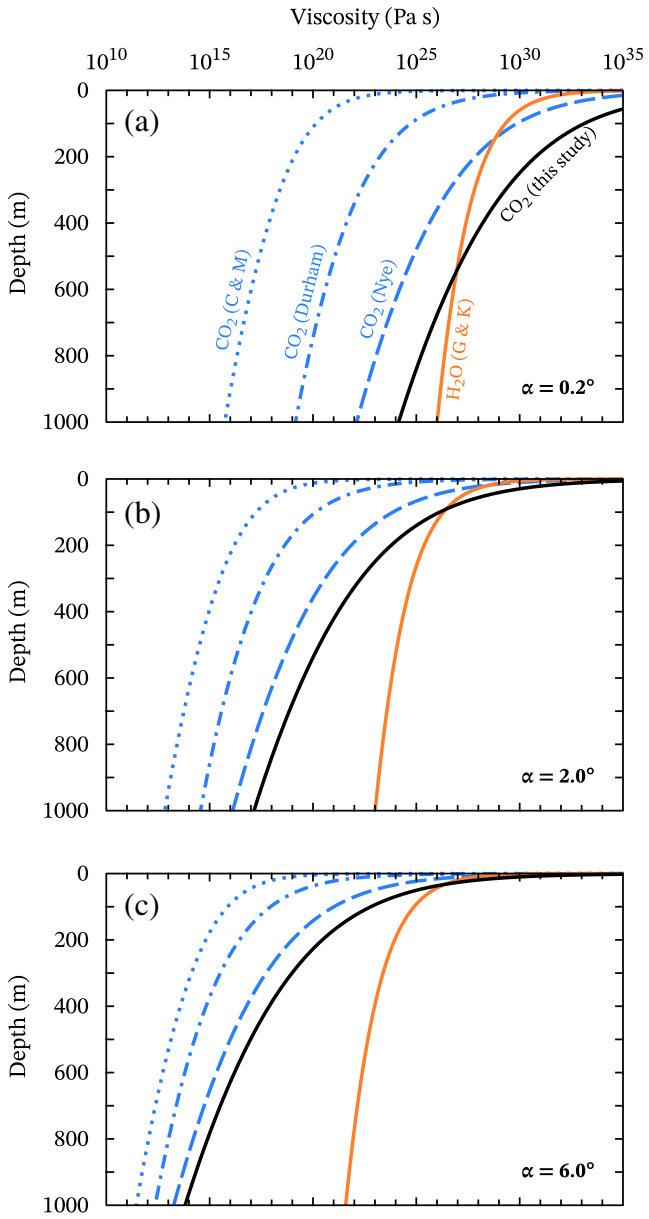

Figure 3. Viscosity as a function of depth through the MCID, calculated using various flow laws for H_2O and CO_2 ice (see Table 1), with surface slopes of (a) 0.2°, (b) 2°, and (c) 6°.

(Brown et al., 2014). However, some experimental work suggests that spectral observations are best matched with grains approaching 1 m in size (Philippe, 2016).

4.2. On the Possibility of Premelting

We observe linear-viscous ($n \approx 1$) deformation only within ~15° of the CO_2 melting temperature. In crystalline materials, marked changes in grain boundary structure (and, thus, material properties) are expected under near-solidus conditions due to equilibrium premelting (Dash et al., 1995) and other forms of "premonitory melting" (Dash et al., 2006; Luo & Chiang, 2008), i.e., subsolidus melting at sites of disordered crystal structure—for example, grain boundaries, subgrain walls, and dislocations (Alsayed et al., 2005; Levine et al., 2016). Notably, premelting is thought to cause an increase in water ice creep rates above −15°C (e.g., Goldsby & Kohlstedt, 2001). The development of water films along grain boundaries can enhance grain-scale stresses and provide short-circuit diffusion pathways (Cooper & Kohlstedt, 1986), raising an interesting question: are we able to observe linear-viscous (diffusion) creep only because grain boundary diffusion is enhanced by subsolidus melting and/or near-solidus grain boundary disordering? If so, we can reasonably speculate that the linear-viscous behavior observed here represents diffusion creep rate-limited by grain boundary diffusion—Coble creep—for which the grain size exponent, m, should equal 3 (Frost & Ashby, 1982). If not, the observed $n \approx 1$ behavior may instead reflect diffusion creep rate-limited by diffusion through grain interiors—Nabarro-Herring creep—for which $m = 2$ (Frost & Ashby, 1982). A test of these models awaits the development of procedures for reliably measuring the grain sizes (and, thus, grain size sensitivity) of deformed CO_2 ice samples.

4.3. Strength of the MCID

We have investigated the rheological behavior of CO_2 ice over a broader range of conditions than previously explored and find evidence for both dislocation creep at high stresses and diffusion creep at low stresses. To examine our findings in the context of MCID flow, and for comparison with previous experimental studies, we calculate viscosity as a function of depth through the CO_2-rich upper kilometer of the SPLD (Figure 3). In the absence of a well-constrained diffusion creep flow law for CO_2 ice, we are presently only able to calculate viscosity arising from dislocation creep ($n = 8$). Nevertheless, we can make direct comparisons to the previous CO_2 flow laws, which, likewise, are defined only for the nonlinear power law creep regime. It is worth reiterating that even though our experimental samples are likely much finer grained than CO_2 ices found within the MCID (Brown et al., 2014; Philippe, 2016), creep within the nonlinear ($n = 8$) regime is expected to be grain-size-insensitive. Indeed, our annealed and fine-grained samples have similar strengths within the nonlinear regime (Figures 2a and S7).

We calculate viscosity as a function of depth through the MCID using a present-day surface temperature of 150 K, with a thermal gradient of 16 K/km based on the thermal conductivity of CO_2 ice (0.63 W/m/K; Ross & Kargel, 1998) and geothermal flux of Mars (~10 mW/m^2; Ojha et al., 2019). Shear stresses τ as a function of depth z were calculated as $\tau(z) = \rho g z \sin\alpha$ (Nye, 1952), with Martian gravitational acceleration $g = 3.711$ m/s^2, and surface slopes of $\alpha = 0.2°$, 2°, and 6° (Figures 1c and 1d). CO_2 density, ρ, was calculated as a function of temperature following Mangan et al. (2017). Shear stresses were converted to equivalent stresses using $\sigma = \sqrt{3}\tau$. For comparison, we also plot viscosity through a 1-km-thick layer of water ice using the composite flow law of Goldsby and Kohlstedt (2001), with a thermal conductivity for water ice of 4 W/m/K at 150 K

(Ross & Kargel, 1998), and $\rho = 920$ kg/m^3. Although the water-ice flow laws of Goldsby and Kohlstedt (2001) incorporate grain-size-dependent creep mechanisms, grain-size-insensitive dislocation creep dominates for all likely grain sizes (1 μm to 1 m).

The CO_2 and H_2O ice flow laws all predict a decrease in viscosity as temperature increases with depth (Figure 3). For gently sloping regions, the various CO_2 ice flow laws predict vastly differing viscosities (Figure 3a), with our $n = 8$ flow law predicting CO_2 ice to be orders of magnitude stronger than previously thought, and stronger even than H_2O ice. However, on the steep flanking slopes of SPLD topographic basins, CO_2 ice viscosity is predicted to decrease dramatically, with the CO_2 flow laws all providing similar viscosity estimates, up to 8–10 orders of magnitude lower than the predicted H_2O ice viscosity (Figure 3b and 3c). This seemingly extreme sensitivity to surface slope—and large degree of variability among the CO_2 ice flow laws, particularly at low surface slopes (i.e., small stresses; Figure 3a)—arises from the strong nonlinearity of the flow laws. Estimates of the stress sensitivity of CO_2 ice creep vary from $n \approx 4$ (Clark & Mullin, 1976) to $n = 8$ (this study); thus, for an order-of-magnitude change in stress, estimated changes in strain rate will differ by up to 4 orders of magnitude. Variability among the flow laws is minimized when surface slope is greater, because the stresses imposed under such conditions are closer to those imposed in the laboratory (i.e., because less extrapolation is required). Nevertheless, even under laboratory conditions our $n = 8$ flow law suggests that CO_2 ice is slightly stronger than previously found (Clark & Mullin, 1976; Durham et al., 1999; Nye et al., 2000)—we attribute this to the difference in impurity content. Overall, however, the highly nonlinear CO_2 flow laws all provide a mechanism for MCID formation, with CO_2 predicted to flow rapidly on the steep flanks of SPLD basins, enabling rapid CO_2 ponding. Once ponded, the MCID are likely topographically constrained by their steep bounding slopes, thereby persisting as thick deposits and preserving a 500-kyr-long south polar climate record.

5. Summary

Recent satellite observations have revealed the presence of massive CO_2 ice deposits (MCID) within the upper kilometer of the otherwise water-ice-rich south polar layered deposits (SPLD) (Bierson et al., 2016; Phillips et al., 2011; Putzig et al., 2018). To shed light on the growing evidence for glacial flow of the MCID, we conducted a series of laboratory deformation experiments on CO_2 ice over a broader range of experimental conditions than previously explored, and with samples of higher purity and finer grain size. Our experiments corroborate previous observations of highly nonlinear creep at large stresses, best described using a power law constitutive equation with the stress exponent $n = 8$. However, at low stresses and high temperatures, we find evidence for a previously unseen, linear-viscous ($n \approx 1$), grain-size-sensitive creep regime. Extrapolation of our $n = 8$ flow law to MCID conditions shows that CO_2 ice is stronger than predicted by previous nonlinear CO_2 flow laws, which were derived from experiments performed on samples containing trace impurities (Clark & Mullin, 1976; Durham et al., 1999). Nevertheless, the flow laws consistently show that CO_2 ice is orders of magnitude weaker than H_2O ice in regions of steep topography (i.e., high shear stress), such that CO_2 ice may flow rapidly into, and pond within, topographic basins of the underlying SPLD, as observed from satellite data (Figure 1b). Further work is required to quantify the grain-size-sensitive creep behavior of CO_2 ice, which may be important in the low-stress upper reaches, and gently sloping regions, of the MCID.

Data Availability Statement

Mechanical data are presented in Table S1 in the supporting information. Steady state mechanical data are available for download from the Woods Hole Open Access Server (https://doi.org/10.26025/1912/26314).

Acknowledgments

This work was funded by NASA grant NNH16ZDA001N-SSW awarded to Smith and Goldsby. Additional salary support for Cross was provided by the WHOI Investment in Science Fund. We thank W. B. Durham and D. Wallis for insightful reviews, and W. B. Durham for various discussions regarding CO_2 ice rheology.

References

Alsayed, A. M., Islam, M. F., Zhang, J., Collings, P. J., & Yodh, A. G. (2005). Chemistry: Premelting at defects within bulk colloidal crystals. *Science*, *309*(5738), 1207–1210. https://doi.org/10.1126/science.1112399

Bierson, C. J., Phillips, R. J., Smith, I. B., Wood, S. E., Putzig, N. E., Nunes, D., & Byrne, S. (2016). Stratigraphy and evolution of the buried CO_2 deposit in the Martian south polar cap. *Geophysical Research Letters*, *43*, 4172–4179. https://doi.org/10.1002/2016GL068457

Brown, A. J., Piqueux, S., & Titus, T. N. (2014). Interannual observations and quantification of summertime H_2O ice deposition on the Martian CO_2 ice south polar cap. *Earth and Planetary Science Letters*, *406*, 102–109. https://doi.org/10.1016/j.epsl.2014.08.039

Chase, S. C., Hatzenbeler, H., Kieffer, H. H., Miner, E., Münch, G., & Neugebauer, G. (1972). Infrared radiometry experiment on Mariner 9. *Science*, *175*(4019), 308–309. https://doi.org/10.1126/science.175.4019.308

Clark, B. R., & Mullin, R. P. (1976). Martian glaciation and the flow of solid CO_2. *Icarus*, *27*(2), 215–228. https://doi.org/10.1016/0019-1035(76)90005-1

Cooper, R. F., & Kohlstedt, D. L. (1986). Rheology and structure of olivine-basalt partial melts. *Journal of Geophysical Research*, *91*(B9), 9315. https://doi.org/10.1029/JB091iB09p09315

Dash, J. G., Fu, H., & Wettlaufer, J. S. (1995). The premelting of ice and its environmental consequences. *Reports on Progress in Physics*, *58*(1), 115. https://doi.org/10.1088/0034-4885/58/1/003

Dash, J. G., Rempel, A. W., & Wettlaufer, J. S. (2006). The physics of premelted ice and its geophysical consequences. *Reviews of Modern Physics*, *78*(3), 695–741. https://doi.org/10.1103/RevModPhys.78.695

de Bresser, J. H. P. (2002). On the mechanism of dislocation creep of calcite at high temperature: Inferences from experimentally measured pressure sensitivity and strain rate sensitivity of flow stress. *Journal of Geophysical Research*, *107*(B12), 2337. https://doi.org/10.1029/2002JB001812

Durham, W. B., Kirby, S. H., & Stern, L. A. (1999). Steady-state flow of solid CO_2: Preliminary results. *Geophysical Research Letters*, *26*(23), 3493–3496. https://doi.org/10.1029/1999GL008373

Frost, H. J., & Ashby, M. F. (1982). *Deformation mechanism maps: The plasticity and creep of metals and ceramics*. Oxford: Pergamon press.

Goldsby, D. L. (2006). Superplastic flow of ice relevant to glacier and ice-sheet mechanics. In *Glacier Science and Environmental Change* (pp. 308–314). Oxford: Blackwell.

Goldsby, D. L., & Kohlstedt, D. L. (2001). Superplastic deformation of ice: Experimental observations. *Journal of Geophysical Research*, *106*(B6), 11,017–11,030. https://doi.org/10.1029/2000JB900336

Heard, H. C., Durham, W. B., Boro, C. O., & Kirby, S. H. (1990). A triaxial deformation apparatus for service at $77 < T < 273$ K. In *The brittle-ductile transition in rocks: The Heard volume*, *Geophysic Monogr. Ser.* (Vol. 56, pp. 225–228). Washington, DC: American Geophysical Union.

Herkenhoff, K. E., & Plaut, J. J. (2000). Surface ages and resurfacing rates of the polar layered deposits on Mars. *Icarus*, *144*(2), 243–253. https://doi.org/10.1006/icar.1999.6287

Herr, K. C., & Pimentel, G. C. (1969). Infrared absorptions near three microns recorded over the polar cap of Mars. *Science*, *166*(3904), 496–499. https://doi.org/10.1126/science.166.3904.496

Hirth, G., & Kohlstedt, D. L. (2015). The stress dependence of olivine creep rate: Implications for extrapolation of lab data and interpretation of recrystallized grain size. *Earth and Planetary Science Letters*, *418*, 20–26. https://doi.org/10.1016/j.epsl.2015.02.013

Kaufmann, E., Attree, N., Bradwell, T., & Hagermann, A. (2020). Hardness and yield strength of CO ice under Martian temperature conditions. *Journal of Geophysical Research: Planets*, *125*, e2019JE006217. https://doi.org/10.1029/2019JE006217

Kuiper, E.-J. N., Weikusat, I., de Bresser, J. H. P., Jansen, D., Pennock, G. M., & Drury, M. R. (2020). Using a composite flow law to model deformation in the NEEM deep ice core, Greenland—Part 1: The role of grain size and grain size distribution on deformation of the upper 2207 m. *The Cryosphere*, *14*(7), 2429–2448. https://doi.org/10.5194/tc-14-2429-2020

Kumar, P., Kassner, M. E., & Langdon, T. G. (2007). Fifty years of Harper–Dorn creep: A viable creep mechanism or a Californian artifact? *Journal of Materials Science*, *42*(2), 409–420. https://doi.org/10.1007/s10853-006-0782-4

Levine, J. S. F., Mosher, S., & Rahl, J. M. (2016). The role of subgrain boundaries in partial melting. *Journal of Structural Geology*, *89*, 181–196. https://doi.org/10.1016/J.JSG.2016.06.006

Luo, J., & Chiang, Y.-M. (2008). Wetting and prewetting on ceramic surfaces. *Annual Review of Materials Research*, *38*(1), 227–249. https://doi.org/10.1146/annurev.matsci.38.060407.132431

Luthy, H., Miller, A. K., & Sherby, O. D. (1980). The stress and temperature dependence of steady-state flow at intermediate temperatures for pure polycrystalline aluminum. *Acta Metallurgica*, *28*(2), 169–178. https://doi.org/10.1016/0001-6160(80)90066-8

Mangan, T. P., Salzmann, C. G., Plane, J. M. C., & Murray, B. J. (2017). CO_2 ice structure and density under Martian atmospheric conditions. *Icarus*, *294*, 201–208. https://doi.org/10.1016/j.icarus.2017.03.012

Manning, C. V., Bierson, C., Putzig, N. E., & McKay, C. P. (2019). The formation and stability of buried polar CO_2 deposits on Mars. *Icarus*, *317*, 509–517. https://doi.org/10.1016/j.icarus.2018.07.021

Marquardt, K., & Faul, U. H. (2018). The structure and composition of olivine grain boundaries: 40 years of studies, status and current developments. In *Physics and Chemistry of Minerals* (Vol. 45, pp. 139–172). Verlag: Springer. https://doi.org/10.1007/s00269-017-0935-9

Nye, J. F. (1952). The mechanics of glacier flow. *Journal of Glaciology*, *2*(12), 82–93. https://doi.org/10.3189/S0022143000033967

Nye, J. F., Durham, W. B., Schenk, P. M., & Moore, J. M. (2000). The instability of a south polar cap on Mars composed of carbon dioxide. *Icarus*, *144*(2), 449–455. https://doi.org/10.1006/ICAR.1999.6306

Ojha, L., Nerozzi, S., & Lewis, K. (2019). Compositional constraints on the north polar cap of Mars from gravity and topography. *Geophysical Research Letters*, *46*, 8671–8679. https://doi.org/10.1029/2019GL082294

Philippe, S. (2016). Microphysique des processus saisonniers des glaces de Mars et Pluton: Suivi par télédétection hyperspectrale et étude expérimentale. Université Grenoble Alpes.

Phillips, R. J., Davis, B. J., Tanaka, K. L., Byrne, S., Mellon, M. T., Putzig, N. E., et al. (2011). Massive CO_2 ice deposits sequestered in the south polar layered deposits of Mars. *Science (New York, N.Y.)*, *332*(6031), 838–841. https://doi.org/10.1126/science.1203091

Plaut, J. J., Picardi, G., Safaeinili, A., Ivanov, A. B., Milkovich, S. M., Cicchetti, A., et al. (2007). Subsurface radar sounding of the south polar layered deposits of Mars. *Science*, *316*(5821), 92–95. https://doi.org/10.1126/science.1139672

Poirier, J. P. (1985). *Creep of crystals: high-temperature deformation processes in metals, ceramics and minerals*. New York: Cambridge University Press.

Putzig, N. E., Smith, I. B., Perry, M. R., Foss, F. J., Campbell, B. A., Phillips, R. J., & Seu, R. (2018). Three-dimensional radar imaging of structures and craters in the Martian polar caps. *Icarus*, *308*, 138–147. https://doi.org/10.1016/j.icarus.2017.09.023

Renner, J., & Evans, B. (2002). Do calcite rocks obey the power-law creep equation? In S. de Meer, M. R. Drury, J. H. P. de Bresser, G. M. Pennock (Eds.), *Deformation mechanisms, rheology and tectonics: Current Status and future perspectives*, *Special publications* (Vol. 200, pp. 293–307). London: Geological Society.

Renner, J., Evans, B., & Siddiqi, G. (2002). Dislocation creep of calcite. *Journal of Geophysical Research*, *107*(B12), 2364. https://doi.org/10.1029/2001JB001680

Ross, R. G., & Kargel, J. S. (1998). Thermal conductivity of solar system ices, with special reference to Martian polar caps. In C. de Bergh, M. Festou, B. Schmitt (Eds.), *Solar System Ices* (pp. 33–62). Dordrecht, Netherlands: Kluwer Academic Publishers. https://doi.org/10.1007/978-94-011-5252-5_2

Ruano, O. A., Miller, A. K., & Sherby, O. D. (1981). The influence of pipe diffusion on the creep of fine-grained materials. *Materials Science and Engineering*, *51*(1), 9–16. https://doi.org/10.1016/0025-5416(81)90100-2

Sagan, C. (1973). Liquid carbon dioxide and the Martian polar laminas. *Journal of Geophysical Research*, *78*(20), 4250–4251. https://doi.org/10.1029/jb078i020p04250

Sherby, O. D., & Weertman, J. (1979). Diffusion-controlled dislocation creep: A defense. *Acta Metallurgica*, *27*(3), 387–400. https://doi.org/10.1016/0001-6160(79)90031-2

Thomas, P. C., James, P. B., Calvin, W. M., Haberle, R., & Malin, M. C. (2009). Residual south polar cap of Mars: Stratigraphy, history, and implications of recent changes. *Icarus*, *203*(2), 352–375. https://doi.org/10.1016/J.ICARUS.2009.05.014

Weertman, J. (1957). Steady-state creep of crystals. *Journal of Applied Physics*, *28*(10), 1185–1189. https://doi.org/10.1063/1.1722604